ACS Photonics

Article

Cite This: ACS Photonics XXXX, XXX, XXX−XXX

Metasurface-Mediated Quantum Entanglement

Pankaj K. Jha,[†,§] Nir Shitrit,[†,§] Jeongmin Kim,[†] Xuexin Ren,[†] Yuan Wang,[†] and Xiang Zhang*[,†,‡]

[†]NSF Nanoscale Science and Engineering Center (NSEC), 3112 Etcheverry Hall, University of California, Berkeley, California 94720, United States

[‡]Materials Sciences Division, Lawrence Berkeley National Laboratory, 1 Cyclotron Road, Berkeley, California 94720, United States

Supporting Information

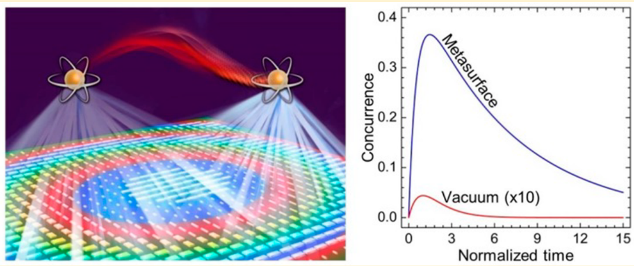

ABSTRACT: Entanglement-based quantum science exploits subtle properties of quantum mechanics into applications such as quantum computing, sensing, and metrology. The emerging route for quantum computing applications, which calls for ultracompact, integrated, and scalable architecture, aims at on-chip entangled qubits. In this context, quantum entanglement among atomic qubits was achieved via cold-controlled collisions which are only significant at subwavelength separations. However, as other manifolds of quantum state engineering require single-site addressability and controlled manipulation of the individual qubit using diffraction-limited optics, entanglement of qubits separated by macroscopic distances at the chip level is still an outstanding challenge. Here, we report a novel platform for on-chip quantum state engineering by harnessing the extraordinary light-molding capabilities of metasurfaces. We theoretically demonstrate quantum entanglement between two qubits trapped on a chip and separated by macroscopic distances, by engineering their coherent and dissipative interactions via the metasurface. Spatially scalable interaction channels offered by the metasurface enable robust generation of entanglement, with large values of concurrence and remarkable revival from sudden death. The metasurface route to quantum state engineering opens a new paradigm for on-chip quantum science and technologies.

KEYWORDS: *metasurfaces, wavefront molding, single-photon operation, quantum entanglement, quantum state engineering*

Quantum state engineering aims at meticulous preparation, control, and manipulation of the quantum states of an atom, ion, photon, etc.[1] It has emerged as a key tool for quantum technology[2] that allows controlling the functionality of a complex system according to the laws of quantum physics. Particularly, quantum states of a many-body system that are nonseparable, i.e., entangled states, exhibit correlations that are beyond the scope of classical realms.[3] Solid-state quantum emitters (quantum dots, color centers, defects in two-dimensional semiconductors, etc.) appear at random positions in complex hosting environments, giving rise to rapid decoherence of their optical transitions. In stark contrast, ultracold atoms benefit from long coherence time and precise trapping methods. As they also benefit from unprecedented control by optical and magnetic fields, two entangled atomic qubits serve as the building block for quantum computation and simulations.[4] While entanglement-based quantum communication targets for remote distances among the qubits, quantum computing aims at on-chip architecture.[5] In the former case, common approaches to entangle atomic qubits use high-*Q* cavity[6] and optical fibers,[7] whereas in the latter, cold-controlled collisions,[8,9] Rydberg blockades,[10] photonic crystal platforms,[11] and plasmonic waveguides[12] are used. However, Rydberg blockade suffers from the challenge of low fidelity due to imperfect blockade; the stringent near-field position requirement of the qubits, which is imperative for achieving a high β factor, is an arduous task in interfacing cold atoms with a photonic crystal platform or plasmonic waveguide, which also lacks spatial scalability to macroscopic distances due to optical (ohmic) losses. On-chip quantum entanglement via cold-controlled collisions among atomic qubits, which are only significant at subwavelength separations, was observed in a microfabricated solid-state device to trap and manipulate cold atoms or ions near an interface.[13] However, quantum entanglement based on this platform[9] still lacks individual qubit addressability[14] and controlled manipulation required by other manifolds of quantum state engineering. We propose to overcome this limitation by harnessing the unique capability of metasurfaces that enables spatially scalable interaction channels.

Photonic metasurfaces are two-dimensional ultrathin arrays of engineered meta-atoms or optical nanoantennas that mold optical wavefronts at subwavelength spatial resolution via phase gradients imparted at their interfaces.[15−17] Metasurfaces are of particular interest, as they revolutionize optical designs by enabling the realization of virtually flat optics via the replacement of bulky optical components with ultrathin planar elements,[15−22] which possess ease-of-fabrication advantages. Up-to-date metasurface applications rely on classical optical fields, where the number of photons is large; however, judiciously designed metasurfaces can also be harnessed for

Received: October 19, 2017
Published: December 1, 2017

DOI: 10.1021/acsphotonics.7b01241
ACS Photonics XXXX, XXX, XXX−XXX

quantum fields at the single-photon level.[23] As gradient metasurfaces offer (i) complete control of the polarization state of the engineered wavefront,[24] (ii) highly efficient light redirection[21,24] from source to target, and (iii) an ultrathin planar platform[16,17] that can be potentially compatible with microscale atom-trapping devices,[25] they provide a promising route for on-chip quantum state engineering of trapped quantum emitters (atoms, ions, etc.). Here, we theoretically demonstrate quantum entanglement at the chip level between two atomic qubits separated by macroscopic distances, where their long-range interaction is mediated by a metasurface.

We considered a system of two identical quantum emitters as qubits with upper levels $|a_\alpha\rangle$ and lower levels $|b_\alpha\rangle$ ($\alpha = 1, 2$). The qubits are located at fixed but arbitrary positions $\mathbf{r}_{1,2}$ such that the distance between them $d \gg \lambda$ and their height from the metasurface $h \gg \lambda$, where λ is the free space wavelength corresponding to the $|a_\alpha\rangle \leftrightarrow |b_\alpha\rangle$ atomic transition. Note that as electromagnetic field fluctuations thwart the trapping of atomic qubits and threaten to decohere their quantum states in the vicinity of a metallic interface,[13] a distant height from the metasurface overcomes these roadblocks, ushering in a feasible experimental platform. In free space, a qubit emits radiation in a 4π solid angle; subsequently, dipole−dipole interaction with another qubit located at a distance $d \gg \lambda$ is negligible. However, in the presence of a prudently designed metasurface, one can engineer strong interactions between two qubits over macroscopic distances by collecting emission from the source qubit and redirecting it toward the target qubit (Figure 1). This interaction induces quantum correlations between the qubits, which play a key role for realizing quantum technologies.

The interaction of the qubits mediated by the metasurface is dictated by the dipole scattered field, i.e., a secondary field of the dipole source that was emitted and then probed at the target position after it was scattered in the environment. As conventional light−metasurface interactions consider plane-wave excitation, we derived a generic platform of a dipole−metasurface interaction for calculating the scattered field. For simplicity, we considered atomic qubits with transition dipole matrix elements that are real and oriented along the same direction; without loss of generality, we choose the y-axis, i.e., $\mathbf{p}_1 = \mathbf{p}_2 = p\hat{y}$. The electric field incident on the metasurface by a point atomic dipole located at $\mathbf{r}_1 = (x_1, y_1, z_1)$ can be calculated via $\mathbf{E}(\mathbf{r}, \mathbf{r}_1, \omega) = \omega^2\mu\mu_0\, \overline{\overline{\mathbf{G}}}(\mathbf{r}, \mathbf{r}_1, \omega)\mathbf{p}_1$, where $\overline{\overline{\mathbf{G}}}$ denotes the dyadic Green's function given by

$$\overline{\overline{\mathbf{G}}} = \frac{e^{ikR}}{4\pi R}\left[\left(1 + \frac{ikR - 1}{k^2R^2}\right)\overline{\overline{\mathbf{I}}} + \frac{3 - 3ikR - k^2R^2}{k^2R^2}\frac{\mathbf{R}\otimes\mathbf{R}}{R^2}\right] \tag{1}$$

Here, $\mathbf{r} = (x, y, 0)$ is the vector position at the metasurface plane, ω is the $|a_\alpha\rangle \leftrightarrow |b_\alpha\rangle$ atomic transition frequency, μ is the relative permeability, μ_0 is the vacuum permeability, $k = 2\pi/\lambda$ is the wavenumber, and $\mathbf{R} = \mathbf{r} - \mathbf{r}_1$. We designed the metasurface such that it imprints a phase profile $\Phi(x, y)$ only to a preselected polarization (chosen as y-polarized light, i.e., E_y) of the incident field $\mathbf{E}(z = 0^+, \mathbf{r}, \omega)$, whereas for other components, the metasurface acts as a mirror (see Supporting Information, section 2 for the polarization-dependent response of the metasurface). Subsequently, we expressed the reflected field just above the metasurface as $\mathbf{E}_r(z = 0^+, \mathbf{r}, \omega) = \sqrt{\eta}(-1, -e^{i\Phi(x,y)}, 1)^T\, \mathbf{E}(z = 0^+, \mathbf{r}, \omega)$, where η is the reflection efficiency (intensity) of the metasurface. Finally, by employing the Huygens−Fresnel diffraction integral,[26] the scattered field at the desired point $\mathbf{r}_2 = (x_2, y_2, z_2)$ can be calculated as

$$\mathbf{E}_s(\mathbf{r}_2, \mathbf{r}_1, \omega) = -i\frac{k}{2\pi}\iint \cos\theta\left(1 + \frac{i}{kr_0}\right)\frac{e^{ikr_0}}{r_0}\mathbf{E}_r(x, y, 0)\,dx\,dy \tag{2}$$

where $r_0 = \sqrt{(x_2 - x)^2 + (y_2 - x)^2 + {z_2}^2}$ and $\cos\theta = h/r_0$ is the inclination factor.

We engineer the quantum states of the two qubits by introducing a designed interface that mediates the interaction between them, so the metasurface role is to redirect the emitted light from the source qubit to the target qubit. Such light bending requires constructive interference between all light paths consisting of propagation from source to interface and from interface to target (see Figure 2a inset). This functionality is optically equivalent to compensation of the phase accumulated via propagation through free space by the phase shift imparted by the metasurface. We consider the positions of the source and target qubits at $\mathbf{r}_1 = (-d/2, 0, h)$ and $\mathbf{r}_2 = (d/2, 0, h)$, respectively. Accordingly, the phase profile imprinted at the metasurface is $\Phi(x,y) = -2\pi/\lambda[\sqrt{(x + d/2)^2 + y^2 + h^2} + \sqrt{(x - d/2)^2 + y^2 + h^2}]$, where x and y are the metasurface coordinates. Note that equal phase lines correspond to curves of ellipses (Figure 2b). We realized this phase profile by a gap plasmon-based gradient metasurface exhibiting highly efficient control of the reflected light.[27] By changing the dimensions of the nanoantenna building block, the phase of the reflected light

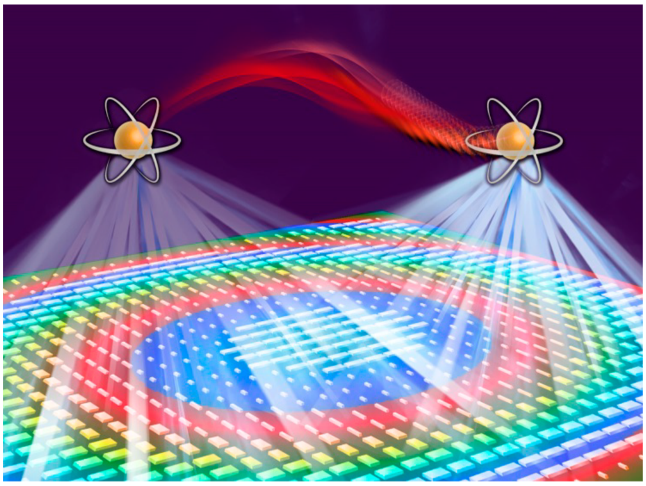

Figure 1. Engineering quantum correlations by interfacing qubits with a metasurface. We considered two trapped atomic qubits that are separated by a macroscopic distance and positioned at a distant height from the metasurface. The two-qubit system is initially prepared in the separable state, where the source qubit (left atom) is in the excited state, while the target qubit (right atom) is in the ground state. We designed a metasurface such that the spontaneous emission from the source qubit is efficiently directed toward the target qubit at the single-photon level. As a result of this interaction, quantum entanglement between the two qubits emerges instantly and lasts much longer than the lifetime of individual qubits. In comparison to the same two atoms in free space, the metasurface interface enables 2 orders of magnitude enhancement in concurrence that quantifies entanglement of a two-qubit system. A false-colored phase distribution, which is mimicked by the metasurface nanoantenna array, spatially molds the flow of light from source to target qubits, resulting in quantum correlations.

DOI: 10.1021/acsphotonics.7b01241
ACS Photonics XXXX, XXX, XXX−XXX

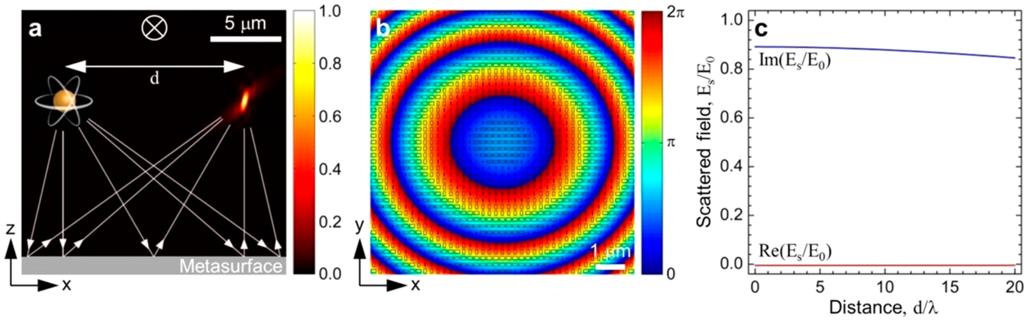

Figure 2. Dipole−metasurface interaction. (a) Simulated scattered field intensity ($|E_y|^2$) distribution for the source atomic dipole located at (-10λ, 0, 20λ) and oriented along the y-axis at the free-space wavelength of λ = 640 nm. The distribution is shown in the $x-z$ plane, where the metasurface lies in the z = 0 plane. With an optimized design, we achieved 82% reflection efficiency (intensity) of the incident field redirected toward the on-demand location (10λ, 0, 20λ). (b) The desired phase profile for molding the incident optical wavefront is presented by the heat map and the corresponding metasurface realization, i.e., silver nanoantenna array, shown on top. We use a set of five nanoantenna phase shifters with the $x-y$ dimensions of (26 nm, 66 nm), (190 nm, 81 nm), (173 nm, 114 nm), (82 nm, 158 nm), and (21 nm, 144 nm), corresponding to 0, $2\pi/5$, $4\pi/5$, $6\pi/5$, and $8\pi/5$ phase shifts, respectively. This realization relies on a gap plasmon-based gradient metasurface with 30 nm nanoantenna thicknesses and a 65 nm dielectric (MgF_2) spacer layer. (c) Dependence of the scattered field (both real and imaginary parts) on the separation d between the source atomic dipole and the target position. A nearly constant high value of the imaginary part of the scattered field is maintained over macroscopic distances $d \gg \lambda$, which is essential for engineering quantum correlations generated with another qubit located at the target point. Note that each point on the curve corresponds to a different metasurface design. The upper limit for the scattered field is E_0, which is the imaginary part of the field induced by the source dipole at its position.

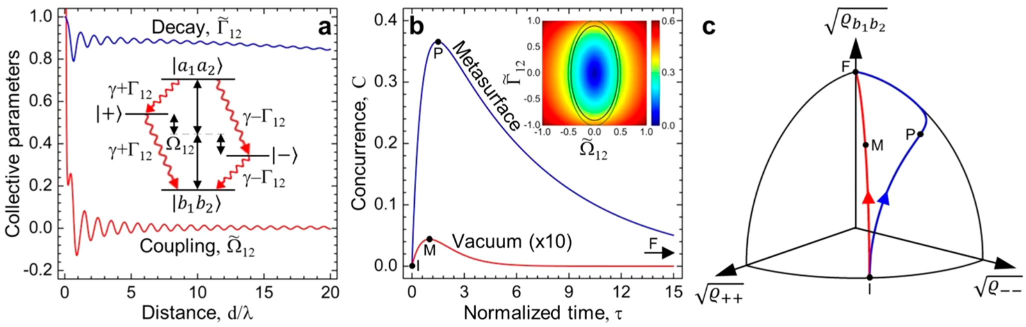

Figure 3. Metasurface-enabled quantum entanglement. (a) Dependence of the collective parameters (coupling and decay) on the separation between the two qubits at a height of 20λ from the metasurface. In the presence of a prudently designed metasurface, strong dissipative interaction between the qubits over macroscopic distances is engineered. The inset shows the equivalent four-level atomic states used to study the dynamics of the two-qubit system. Note that the symmetric ($|+\rangle$) and asymmetric ($|-\rangle$) states decay at enhanced ($\gamma + \Gamma_{12}$) and suppressed ($\gamma - \Gamma_{12}$) rates, respectively. $\tilde{\Omega}_{12} = \Omega_{12}/\gamma$ and $\tilde{\Gamma}_{12} = \Gamma_{12}/\gamma$ are the normalized collective parameters (see Supporting Information, section 3, for the normalizing factor of the spontaneous emission decay rate γ). (b) Time evolution of the concurrence for the two-qubit system separated by a macroscopic distance of $d = 20\lambda$ and initially prepared in the separable state $|\psi_{12}(0)\rangle = |a_1\rangle \otimes |b_2\rangle$. Note that this initial state corresponds to $\varrho_{++}(0) = \varrho_{--}(0) = \varrho_{+-}(0) = 0.5$. In the presence of the metasurface (blue line), the maximum value of concurrence is 0.366, which is 2 orders of magnitude higher than a vacuum (red line). The heat map in the inset shows the maximum value of concurrence in the collective parameters space. Green and black lines denote equal maximum concurrence lines of lossless and actual metasurfaces, respectively. (c) Time evolution of the populations of the symmetric and asymmetric states and the ground state ($|b_1\rangle \otimes |b_2\rangle$) on the population sphere defined as $(\sqrt{\varrho_{++}})^2 + (\sqrt{\varrho_{--}})^2 + (\sqrt{\varrho_{b_1b_2}})^2 = 1$. The dots I and F are the initial and final points, respectively, while the maximum of concurrence occurs at P for the metasurface (blue line) and at M in a vacuum (red line). The arrows show the evolution of time.

is molded to span the entire 2π phase range.[27] We mimicked the desired phase profile by a set of five different silver nanoantenna phase shifters, yielding 82% reflection efficiency of the constructed metasurface (see Supporting Information, section 1, for the detailed metasurface design). By applying the reported method of dipole−metasurface interaction, we obtained the distribution of the scattered field intensity for a y-polarized source dipole, where the efficient light redirection via the metasurface to the target position is evident (Figure 2a). The real and imaginary parts of the scattered field at varying target positions were also calculated to reveal that the scattered field governed by the metasurface is robust over macroscopic dipole separations (Figure 2c). We designed the phase profile of the metasurface such that the real part of the scattered field is suppressed while the imaginary part is enhanced; by considering a finite size metasurface, the ohmic loss due to the metal, and the phase discretization loss,[20] we achieved that ~80% of the dipole source emission is redirected to the target qubit.

The interaction between the source and target qubits mediated via the metasurface is characterized by the spontaneous emission decay rate of the source qubit γ and the collective parameters of decay and coupling rates. The collective damping rate $\Gamma_{12}(\mathbf{r}_1, \mathbf{r}_2)$ quantifies the decay rate of a qubit located at the position $\mathbf{r}_1$ due to the presence of a second qubit positioned at $\mathbf{r}_2$; similarly, the collective coupling rate $\Omega_{12}(\mathbf{r}_1, \mathbf{r}_2)$ quantifies the coherent interaction between the two qubits, resulting in the energy shift of the collective qubit states

DOI: 10.1021/acsphotonics.7b01241
ACS Photonics XXXX, XXX, XXX−XXX

(Figure 3a inset). These parameters are governed by the scattered field at the location of the target qubit, which is controlled by tailoring the optical response of the metasurface interface (see Supporting Information, section 3, for the detailed discussion; note that the inherent decay rate of the source qubit in the presence of the metasurface is similar to the decay rate in free space for macroscopic separations between the qubits). Figure 3a shows the dependence of the collective parameters of decay and coupling on the separation between the qubits, which reveals a strong dissipative interaction.

Entanglement between the two qubits can be quantified by the parameter concurrence.[28] The range of concurrence C varies from 0 (no entanglement) to 1 (maximally entangled). To study the dynamics of a coupled two-qubit system, we employed the collective (Dicke) states, $|u\rangle = |a_1\rangle \otimes |a_2\rangle$, $|\pm\rangle = \frac{1}{\sqrt{2}}\left(|a_1\rangle \otimes |b_2\rangle \pm |b_1\rangle \otimes |a_2\rangle\right)$, $|l\rangle = |b_1\rangle \otimes |b_2\rangle$ with the corresponding energies $2\hbar\omega$, $\hbar(\omega \pm \Omega_{12})$, and 0, where $\hbar$ is the reduced Planck's constant (see the four-level atomic states in Figure 3a inset). Note that the symmetric and asymmetric entangled states are manifested by different decay rates of $\gamma \pm \Gamma_{12}$, respectively. We analyzed spontaneous creation of quantum entanglement between two distant qubits ($d \gg \lambda$) which are oriented along the y-axis and initially prepared in a separable state $|\psi_{12}(0)\rangle = |a_1\rangle \otimes |b_2\rangle$. Such an initial two-qubit state corresponds to a source qubit prepared in the excited state $|a_1\rangle$ and target qubit in the ground state $|b_2\rangle$. In terms of the Dicke states, the time evolution of the concurrence is given by[29] $C(t) = \sqrt{[\varrho_{++}(t) - \varrho_{--}(t)]^2 + 4[\mathrm{Im}(\varrho_{+-})]^2}$, where $\varrho_{++} = \varrho_{++}(0)e^{-(\gamma+\Gamma_{12})t}$ and $\varrho_{--} = \varrho_{--}(0)e^{-(\gamma-\Gamma_{12})t}$ are the populations of the symmetric $|+\rangle$ and asymmetric $|-\rangle$ states, respectively, while $\mathrm{Im}(\varrho_{+-}) = \varrho_{+-}(0)e^{-\gamma t}\sin(2\Omega_{12}t)$ quantifies the coherence between them.[29]

Figure 3b presents the time evolution of the concurrence for the two-qubit system for macroscopic separation and a height of $d = h = 20\lambda$ (see Figure 3c for the corresponding time evolution of the populations of the atomic states). An instant emergence of entanglement ($C > 0$) that builds up to $C_{max} = 0.366$ is clearly seen. Note that in the ideal limit of a lossless and infinitely large metasurface $\Gamma_{12} = \gamma$, which yields that the decay of the asymmetric state is zero, so one can spontaneously generate steady-state entanglement with concurrence $C = 0.5$. In the absence of the metasurface, the maximum concurrence between the same two qubits is $C_{max} = 0.004$, which is about 2 orders of magnitude smaller than the metasurface case. The heat map in Figure 3b inset presents the maximum concurrence as a function of both the collective decay and coupling. For a macroscopic separation between the qubits, the dissipative nature of the collective parameters corresponds to predominant imaginary and suppressed real parts of the scattered field via the metasurface design; more specifically, $\Gamma_{12} \propto \mathrm{Im}(E_s)$ and $\Omega_{12} \propto -\mathrm{Re}(E_s)/2$. Since the real and imaginary parts of the scattered field are also related through energy (intensity) conservation, they form an ellipse contour in the collective parameters space (see green and black curves in Figure 3b inset, which correspond to ideal and actual metasurfaces, respectively). Therefore, suppressing the real part while enhancing the imaginary part of the scattered field offers a route to maximize the entanglement. Moreover, the entanglement performance of the metasurface platform reported here exhibits clear advantages with respect to a plasmonic waveguide,[12] which are (i) immunity from the stringent plasmonic near-field position requirement of the atomic qubits for a feasible experimental demonstration and (ii) enhanced maximum concurrence (see Supporting Information, section 4, for the detailed comparison). Note that metasurfaces and waveguides are fundamentally different interaction channels; the reported metasurface is a designed reflective interface mediating the interaction between the qubits, whereas the interaction channel in a waveguide is a guided mode propagating between the qubits.[12,30−32]

The robustness of entanglement between the qubits is analyzed in Figure 4a via the dependence of maximum

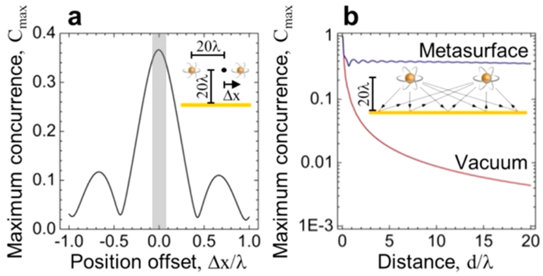

Figure 4. Robust and spatially scalable quantum entanglement between two atomic qubits. (a) Dependence of the maximum concurrence on the position offset $\Delta x/\lambda$ of the target qubit. As shown in the inset, the position of the source qubit is fixed at $(-10\lambda, 0, 20\lambda)$, while that of the varying target qubit is $(10\lambda + \Delta x, 0, 20\lambda)$. The gray-shaded area corresponds to previously reported experimental position tolerances of $\sim 0.08\lambda$ for a trapped atom. Within this position tolerance, the change in the maximum concurrence in the presence of the metasurface is small (~6%). (b) Maximum concurrence as a function of the normalized separation d/λ between the qubits for a vacuum (red line) and metasurface (blue line). The qubits are initially prepared in the separable state $|\psi_{12}(0)\rangle = |a_1\rangle \otimes |b_1\rangle$. When the qubits are separated by a distance $d \ll \lambda$, the interaction is dominated by the collective coupling Ω_{12}. However, for distances $d \approx \lambda$ and beyond, the metasurface maintains the entanglement by enabling strong collective dissipative interaction over macroscopic distances, while in a vacuum, the entanglement dies off quickly. Note that each point on the blue curve corresponds to a different metasurface design.

concurrence against the position offset of the target qubit with respect to its ideal position. Atomic qubits were experimentally trapped at the desired location with position tolerances to a few tens of nanometers by either electric and magnetic potentials created by microscale atom-trapping devices[25] or optical dipole potentials.[33] The maximum concurrence decreases once an offset is introduced; however, this change is not abrupt, and the variation is within ~6% of the optimal value in the shaded region corresponding to the position uncertainty demonstrated in experiments. Figure 4b shows the maximum value of concurrence of the two-qubit system versus the separation between the qubits. As expected, in the regime $d \ll \lambda$, the responses in a vacuum and in the presence of a metasurface are nearly identical. However, there is an abrupt decrease in the maximum concurrence in the regime $d \sim \lambda$, which continues to fall in a vacuum; in stark contrast with the metasurface, a constant value is achieved over 20λ. The upper limit to the distance between the qubits is fundamentally limited by the photonic coherence length, which can go up to meter length scales. The robustness of the metasurface-enabled entanglement over macroscopic separations is a peculiar advantage of the metasurface platform with respect to others (see Supporting Information, section 4, for the plasmonic waveguide comparison).

DOI: 10.1021/acsphotonics.7b01241
ACS Photonics XXXX, XXX, XXX−XXX

Quantum entanglement is quite fragile and prone to degradation owing to deleterious effects of irreversible interactions with the environment.[3] In some scenarios, the decay is sudden (i.e., the concurrence goes to zero at a finite time) rather than asymptotic, a phenomena known as entanglement sudden death.[34] Quantum entanglement can be revived from death in the presence of a dissipative dipole–dipole interaction ($d \ll \lambda$) in a two-qubit system without any external coherent field,[29] where the magnitude of revival depends on the strength of the interaction between the qubits. Figure 5 shows the time evolution of the concurrence, where the sudden death of entanglement is clearly seen (see Supporting Information, section 5, for the detailed analysis). As evident from Figure 3a, a strong interaction between two qubits over macroscopic separations is achieved with a prudently designed metasurface, in contrast to vacuum. Subsequently, the metasurface remarkably revives quantum entanglement even when the qubits are separated by a distance of 20λ (see Supporting Information, Figure S5, for the sudden death without revival by a plasmonic waveguide).

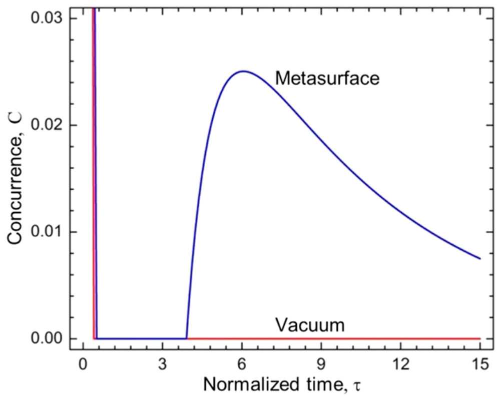

Figure 5. Metasurface-enabled revival of quantum entanglement from sudden death over macroscopic distances. Time evolution of the concurrence for a two-qubit system initially prepared in a nonmaximal entangled state $|\Psi_{12}(0)\rangle = \sqrt{\kappa}(|a_1\rangle \otimes |a_2\rangle) + \sqrt{1-\kappa}(|b_1\rangle \otimes |b_2\rangle)$ with κ = 0.9 in a vacuum (red line) and in the presence of a metasurface (blue line); here, the separation between the two qubits is 20λ. In both cases, the concurrence abruptly vanishes (i.e., sudden death of entanglement); however, it only revives with a mediating metasurface with a death time of $\tau = \gamma t \approx 4$. After the revival, the concurrence grows and eventually decays to zero on a time scale much longer than the lifetime of the qubits. This revival stems from finite collective damping $\tilde{\Gamma}_{12}$ = 0.85 even at a macroscopic distance of 20λ between the qubits.

In summary, we reported on a metasurface-enabled on-chip quantum entanglement over macroscopic distances. The metasurface platform for on-chip quantum state engineering offers a promising route in scaling from two-qubit to many-body entanglement by introducing a multifunctional metasurface.[22] Moreover, as this metasurface enables photonic multitasking, optical trapping of the qubits can be assigned as an additional independent functionality to the primary task of manipulating the flow of photons. Although a microscale atom trapping device platform[13] has already been proven extremely valuable in quantum state engineering,[1] the exquisite control provided by metasurfaces may usher in even more dramatic advances in quantum technologies. Specifically, by bringing the mature metasurface platform to the atom physics community, the reported concept may pave the way for the integration of high-end custom-designed ultrathin optical elements in micro-scale atom-trapping devices for enabling nanoscale quantum optics on a chip.

■ ASSOCIATED CONTENT

Supporting Information

The Supporting Information is available free of charge on the ACS Publications website at DOI: 10.1021/acsphotonics.7b01241.

Metasurface design, polarization-dependent response of the metasurface, derivation of the collective parameters, comparison of entanglement performance between metasurface and plasmonic waveguide platforms, and comparison of revival of quantum entanglement from sudden death between metasurface and plasmonic waveguide platforms (PDF)

■ AUTHOR INFORMATION

Corresponding Author

*E-mail: xiang@berkeley.edu.

ORCID

Xiang Zhang: 0000-0002-3272-894X

Author Contributions

[§]P. K. Jha and N. Shitrit contributed equally to this work.

Notes

The authors declare no competing financial interest.

■ ACKNOWLEDGMENTS

This work was supported by the U.S. Department of Energy, Office of Science, Basic Energy Sciences, Materials Sciences and Engineering Division under Contract No. DE-AC02-05-CH11231 within the Subwavelength Metamaterials Program (KC12XZ) for design and analysis. Support was also provided by Samsung Electronics for simulation.

■ REFERENCES

(1) Ye, J.; Kimble, H. J.; Katori, H. Quantum state engineering and precision metrology using state-insensitive light traps. *Science* **2008**, *320*, 1734−1738.
(2) Dowling, J. P.; Milburn, G. J. Quantum technology: The second quantum revolution. *Philos. Trans. R. Soc., A* **2003**, *361*, 1655−1674.
(3) Horodecki, R.; Horodecki, P.; Horodecki, M.; Horodecki, K. Quantum entanglement. *Rev. Mod. Phys.* **2009**, *81*, 865−942.
(4) Bloch, I.; Dalibard, J.; Nascimbene, S. Quantum simulations with ultracold quantum gases. *Nat. Phys.* **2012**, *8*, 267−276.
(5) Ladd, T. D.; Jelezko, F.; Laflamme, R.; Nakamura, Y.; Monroe, C.; O'Brien, J. L. Quantum computers. *Nature* **2010**, *464*, 45−53.
(6) Hagley, E.; Maître, X.; Nogues, G.; Wunderlich, C.; Brune, M.; Raimond, J. M.; Haroche, S. Generation of Einstein-Podolsky-Rosen pairs of atoms. *Phys. Rev. Lett.* **1997**, *79*, 1−5.
(7) Moehring, D. L.; Maunz, P.; Olmschenk, S.; Younge, K. C.; Matsukevich, D. N.; Duan, L. M.; Monroe, C. Entanglement of single-atom quantum bits at a distance. *Nature* **2007**, *449*, 68−71.
(8) Jaksch, D.; Briegel, H.-J.; Cirac, J. I.; Gardiner, C. W.; Zoller, P. Entanglement of atoms via cold controlled collisions. *Phys. Rev. Lett.* **1999**, *82*, 1975−1978.
(9) Riedel, M. F.; Bohi, P.; Li, Y.; Hansch, T. W.; Sinatra, A.; Treutlein, P. Atom-chip-based generation of entanglement for quantum metrology. *Nature* **2010**, *464*, 1170−1173.
(10) Wilk, T.; Gaetan, A.; Evellin, C.; Wolters, J.; Miroshnychenko, Y.; Grangier, P.; Browaeys, A. Entanglement of two individual neutral atoms using Rydberg blockade. *Phys. Rev. Lett.* **2010**, *104*, 010502.

(11) Goban, A.; Hung, C.-L.; Hood, J. D.; Yu, S.-P.; Muniz, J. A.; Painter, O.; Kimble, H. J. Superradiance for atoms trapped along a photonic crystal waveguide. *Phys. Rev. Lett.* **2015**, *115*, 063601.
(12) Gonzalez-Tudela, A.; Martin-Cano, D.; Moreno, E.; Martin-Moreno, L.; Tejedor, C.; Garcia-Vidal, F. J. Entanglement of two qubits mediated by one-dimensional plasmonic waveguides. *Phys. Rev. Lett.* **2011**, *106*, 020501.
(13) Reichel, J.; Vuletić, V., Eds. *Atom Chips*; Wiley, 2011.
(14) Bakr, W. S.; Gillen, G. I.; Peng, A.; Folling, S.; Greiner, M. A quantum gas microscope for detecting single atoms in a Hubbard-regime optical lattice. *Nature* **2009**, *462*, 74−77.
(15) Bomzon, Z.; Biener, G.; Kleiner, V.; Hasman, E. Space-variant Pancharatnam-Berry phase optical elements with computer-generated subwavelength gratings. *Opt. Lett.* **2002**, *27*, 1141−1143.
(16) Kildishev, A. V.; Boltasseva, A.; Shalaev, V. M. Planar photonics with metasurfaces. *Science* **2013**, *339*, 1232009.
(17) Yu, N.; Capasso, F. Flat optics with designer metasurfaces. *Nat. Mater.* **2014**, *13*, 139−150.
(18) Shitrit, N.; Bretner, I.; Gorodetski, Y.; Kleiner, V.; Hasman, E. Optical spin Hall effects in plasmonic chains. *Nano Lett.* **2011**, *11*, 2038−2042.
(19) Yu, N.; Genevet, P.; Kats, M. A.; Aieta, F.; Tetienne, J.-P.; Capasso, F.; Gaburro, Z. Light propagation with phase discontinuities: Generalized laws of reflection and refraction. *Science* **2011**, *334*, 333−337.
(20) Hasman, E.; Kleiner, V.; Biener, G.; Niv, A. Polarization dependent focusing lens by use of quantized Pancharatnam-Berry phase diffractive optics. *Appl. Phys. Lett.* **2003**, *82*, 328−330.
(21) Khorasaninejad, M.; Chen, W. T.; Devlin, R. C.; Oh, J.; Zhu, A. Y.; Capasso, F. Metalenses at visible wavelengths: Diffraction-limited focusing and subwavelength resolution imaging. *Science* **2016**, *352*, 1190−1194.
(22) Maguid, E.; Yulevich, I.; Veksler, D.; Kleiner, V.; Brongersma, M. L.; Hasman, E. Photonic spin-controlled multifunctional shared-aperture antenna array. *Science* **2016**, *352*, 1202−1206.
(23) Jha, P. K.; Ni, X.; Wu, C.; Wang, Y.; Zhang, X. Metasurface-enabled remote quantum interference. *Phys. Rev. Lett.* **2015**, *115*, 025501.
(24) Arbabi, A.; Horie, Y.; Bagheri, M.; Faraon, A. Dielectric metasurfaces for complete control of phase and polarization with subwavelength spatial resolution and high transmission. *Nat. Nanotechnol.* **2015**, *10*, 937−943.
(25) Folman, R.; Kruger, P.; Schmiedmayer, J.; Denschlag, J.; Henkel, H. Microscopic atom optics: From wires to an atom chip. *Adv. At., Mol., Opt. Phys.* **2002**, *48*, 263−356.
(26) Jackson, J. D. *Classical Electrodynamics*, 2nd ed.; Wiley, 1975.
(27) Pors, A.; Albrektsen, O.; Radko, I. P.; Bozhevolnyi, S. I. Gap plasmon-based metasurfaces for total control of reflected light. *Sci. Rep.* **2013**, *3*, 2155.
(28) Wootters, W. K. Entanglement of formation of an arbitrary state of two qubits. *Phys. Rev. Lett.* **1998**, *80*, 2245−2248.
(29) Ficek, Z.; Tanas, R. Dark periods and revivals of entanglement in a two-qubit system. *Phys. Rev. A: At., Mol., Opt. Phys.* **2006**, *74*, 024304.
(30) Zheng, H.; Baranger, H. U. Persistent quantum beats and long-distance entanglement from waveguide-mediated interactions. *Phys. Rev. Lett.* **2013**, *110*, 113601.
(31) Lee, C.; Tame, M.; Noh, C.; Lim, J.; Maier, S. A.; Lee, J.; Angelakis, D. G. Robust-to-loss entanglement generation using a quantum plasmonic nanoparticle array. *New J. Phys.* **2013**, *15*, 083017.
(32) Gonzalez-Ballestero, C.; Gonzalez-Tudela, A.; Garcia-Vidal, F. J.; Moreno, E. Chiral route to spontaneous entanglement generation. *Phys. Rev. B: Condens. Matter Mater. Phys.* **2015**, *92*, 155304.
(33) Wong-Campos, J. D.; Johnson, K. G.; Neyenhuis, B.; Mizrahi, J.; Monroe, C. High-resolution adaptive imaging of a single atom. *Nat. Photonics* **2016**, *10*, 606−610.
(34) Yu, T.; Eberly, J. Sudden death of entanglement. *Science* **2009**, *323*, 598−601.

DOI: 10.1021/acsphotonics.7b01241
ACS Photonics XXXX, XXX, XXX−XXX